UDC 621.372.413

APPROXIMATE MODEL OF SOLID-STATE COMPONENTS OF TELECOMMUNICATION SYSTEMS

Elena V. Guseva

National Technical University of Ukraine "KPI", Kyiv, Ukraine

A simple electrical model of the solid-state object under investigation as an initial approximation for the problems of tomographic reconstruction and design of telecommunication systems components is proposed. The electrical circuit equivalent to the composition of uniform triangular finite elements has been obtained. Calculations of the equivalent parameters of the solid-state structures are carried out. It is shown that the electrical model proposed displays the properties of solid-state object under study in solving the direct problem qualitatively correct and allows obtaining an analytical solution of the inverse problem.

Introduction

The modern telecommunication systems incorporate a number of functional units that provide transmission, reception and processing of information such as different types of transmission lines, filters, amplifiers, phase-shifters, signal converters. For construct of compact and small cost devices, the solid-state (integral) structures are exclusively used [1, 2]. An industrial production of solid-state components involves the use of nondestructive testing facilities for quality evaluation of used material, detecting its imperfections and finding the discontinuities in it. These measures are carried out in order to prevent the failures of solid-state equipment under manufacturing and to improve its reliability [3]. To investigate the interior structures of materials having a certain degree of conductivity, the methods based on experimental measurements of impedance distribution inside the solid-state object under study are most widely used [4–9]. An application of nondestructive testing facilities is associated with the solution of reconstruction problem of internal structures of solid-state objects in accordance with the results of multi-position measurements on their outer contours. For this purpose, an electric current is energized through the object under investigation, and the values of potentials difference between various points of its surface are measured [6]. An array of experimental values obtained is processed in a computer creating an image (tomogram) of the distribution of impedance, conductance or permittivity of material inside the object [7].

The existing measurement systems such as the industrial computer tomography devices differ in types of information carriers and in element bases used depending on the form and size of the objects under investigation [8–10]. The industrial computer tomography as a non-destructive technology for volume data generation offers the possibility of complete inspection of complex industrial objects. This allows investigating the solid-state structures taking into account all outer and inner geometric features. Thus, the computer impedance tomography is well suited for different kinds of industrial applications [9–11].

In recent years, the requirements to industrially applicable computer impedance tomography relating to image processing have significantly increased. For realization of modern production processes and obtaining of high quality products, it is necessary to optimize manufacture using accurate models of solid-state materials. Therefore, the development of existing methods and search of new ways of adequate image reconstruction can be indicate as very important problems of impedance tomography technology.

An expansion of areas of the practical application of the problem of tomographic reconstruction of physical field distributions inside the solid-state object became possible because of rapid development of computer technology. It allows creating and applying new high-speed methods for processing of information originating from measuring devices.

To obtain the required electrical characteristics of solid-state components, the methods of their design based on appropriate mathematical models must be used. The development of adequate mathematical models and their subsequent implementation in the form of algorithms and programs are associated with the use of methods of the experimental estimation of the obtained results accuracy.

The theoretical image reconstruction by the method of electrical impedance tomography is a difficult mathematical problem. The solution of this tomographic problem allows us to restore the parameters of the solid-state objects under investigation by integral data coming from the measuring lines. Usually, the

number of measuring lines is significantly smaller than the number of researched field components. As a result, the number of unknowns exceeds the number of equations that are formed at the problem solution. Therefore, the image reconstruction of the distribution of the investigated parameters according to incomplete integral data is related to ill-posed problems of electrical impedance tomography [12].

There are a large number of algorithms used for restoring information on parameters of the distributed physical fields. These algorithms are based on optimization techniques and require a considerable amount of computational resources. When using optimization, the design time is highly dependent on the accuracy of the initial approximation.

Reconstruction of the impedance distribution inside the solid-state object under study by measured potentials on its surface is an inverse problem of tomography. The solution process of the inverse problem is iterative. The success of the inverse problem solution depends on the decision accuracy of the direct problem at each step of iterative process as well as on the initial approximation of parameters to be optimized [13].

The purpose of this paper is to propose the simple electrical model of the solid-state object under investigation applicable for defining initial approximation for the problems of tomographic image reconstruction and design of telecommunications systems components.

Electric circuit of the investigated cross section of the solid-state structure

In the experimental study of solid-state objects, the information taken from electrodes placed on the object boundary is usually used. The number of electrodes is determined by size and structure composition of the object under investigation as well as by the required accuracy of results to be obtained, and it is usually equal to $M = 8, 16, 32$. The harmonic probing current of given value is delivered to one of the electrodes. Another one electrode is grounded. The amplitudes of the potentials at all remaining electrodes must be determined. When solving the direct problem, the amplitudes of these potentials are calculated, whereas at solution of the inverse problem they are measured or are specified.

An example of the model of an elementary cell of the solid-state structure under study, on the outer boundary of which $M = 8$ nodes (electrodes) are placed, is shown in Fig. 1, where the central node has the number $M + 1 = 9$. The probing electric current with the amplitude $\dot{I}_m$ is delivered to electrode with the number $m = 1$, whereas the diametrically opposite electrode with the number $n = m + M/2$ is grounded (has zero potential). For the short description of problem considered, we will call this model as a phantom.

The internal cross section of the phantom is divided into eight ($M = 8$) triangular finite elements of equal size. In the general case, each element is characterized by the conductivity σ_i and relative permittivity ε'_i ($i = 1, \ldots, M$), which are assumed as a constant within each finite element.

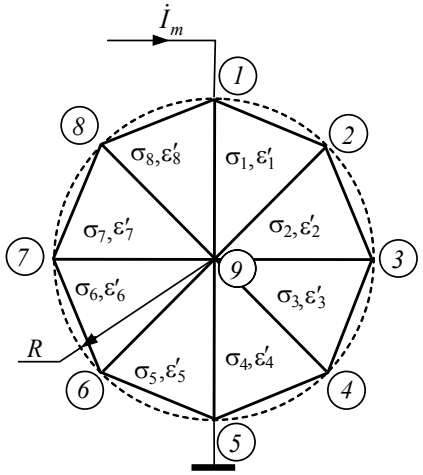

Fig. 1. The internal cross section model of the elementary cell of solid-state structure under investigation.

Dividing the phantom onto a greater number of finite elements, we can obtain a better approximation to the shape of the real crystal structure. This allows taking into account a difference in the electrical parameters of the finite elements more correctly. Parameters of finite elements and their combination are defined by employing the technique described in [14].

Phantom, shown in Fig. 1, can be described by an equivalent electrical circuit shown in Fig. 2.

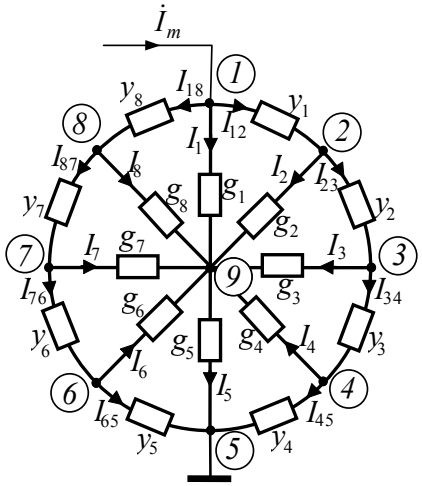

Fig. 2. The electrical circuit of the phantom.

In the general case, each element of this scheme at given frequency is the complex conductivity, which active and reactive components are determined by the

electrical parameters of the finite elements of the phantom shown in Fig. 1. An investigation of the behavior of active and reactive components of the complex conductivity as a function of frequency allows us to define more accurately the equivalent circuit for each element in Fig. 2, and hence correctly reconstruct the phantom (Fig. 1).

For real objects, the unit cell of solid-state structure can be represented by the idealized scheme in the form of complex impedance $\dot{Z} = R - jX$ (Fig. 3*a*) or complex conductivity $\dot{Y} = G + jB$ (Fig. 3*b*) [2, 9].

The concept of complex impedance is based on the idea that each element of the charge should consistently go through the resistive element R and a reactive (capacitive) element X of the structure. Determination of the complete conductivity of the unit cell is based on the assumption that the total moving charge is equal to the sum of the charges flowing through both elements G and B.

In the cases of low and average hardness of the materials under investigation, the typical schemes of the unit cells of solid-state structure can be represented as shown in Fig. 4 [6, 9]. In these schemes, the reactive element S represents predominantly the polarization phenomena, the physical capacity of the unit cell, and some active processes. The resistive element P embodies the electrical permittivity caused by the active processes and represents the energy dissipative components. The element A is an additional resistance which can be interpreted as the purely physical impedance of the solid-state environment.

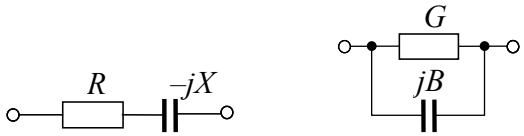

Fig. 3. Idealized schemes of unit cells of solid-state structure.

For adequate representation of the various processes and phenomena occurring in solid-state objects, the more complex electric schemes are developed. Their parameters are determined by analyzing of changes in the frequency range of active and reactive components of the idealized complex resistance or conductance shown in Fig. 3.

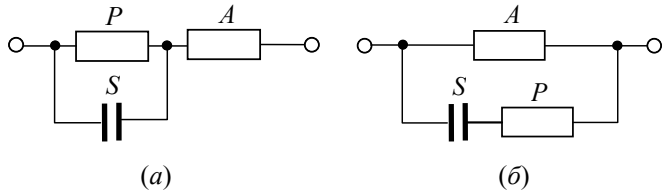

Fig. 4. Typed circuit unit cells of the solid state structure.

To determine the values of all complex conductivities required for the representation of the phantom (Fig. 1) by the equivalent circuit shown in Fig. 2, we take into account the principle of minimum potential energy in a transmission line corresponding to the minimum of stored energy [14]. As a result, we obtain the following expressions:

$$\dot{y}_i = R\frac{\dot{G}_i}{2}\cot\frac{2\pi}{M},\ (i = 1,2,\ldots,M) \tag{1}$$

for finding the conductivities in the outer branches, and

$$\begin{aligned} \dot{g}_1 &= R\frac{\dot{G}_M + \dot{G}_1}{2}\tan\frac{\pi}{M}; \\ \dot{g}_i &= R\frac{\dot{G}_{i-1} + \dot{G}_i}{2}\tan\frac{\pi}{M}, \quad (i = 2,3,...,M) \end{aligned} \tag{2}$$

for determining the conductivities in the internal branches, where $\dot{G}_i = \sigma_i + j\omega\varepsilon_0\varepsilon_i'$ $(i = 1,2,\ldots,M)$.

The solution of direct problem

The solution of direct problem involves the calculation of the potentials amplitudes in the external nodes under influence on the phantom of the harmonic probing current of given amplitude by using the known distribution of specific conductivity on the square of the solid-state object under investigation. The potentials amplitudes in the nodes are defined by the method of nodal potentials. As a result, we obtain a complete matrix of conductivities for the scheme shown in Fig. 2

$$[M_Y] = \begin{bmatrix} \dot{Y}_{11} & -\dot{y}_1 & \cdots & 0 & -\dot{y}_M & -\dot{g}_1 \\ -\dot{y}_1 & \dot{Y}_{22} & \cdots & 0 & 0 & -\dot{g}_2 \\ \vdots & \vdots & \ddots & \vdots & \vdots & \vdots \\ 0 & 0 & \cdots & \dot{Y}_{M-1,M-1} & -\dot{y}_{M-1} & -\dot{g}_{M-1} \\ -\dot{y}_M & 0 & \cdots & -\dot{y}_{M-1} & \dot{Y}_{M,M} & -\dot{g}_M \\ -\dot{g}_1 & -\dot{g}_2 & \cdots & -\dot{g}_{M-1} & -\dot{g}_M & \sum_{i=1}^{M}\dot{g}_i \end{bmatrix},$$

$\dot{Y}_{11} = \dot{g}_1 + \dot{y}_M + \dot{y}_1$; $\dot{Y}_{ii} = \dot{g}_i + \dot{y}_{i-1} + \dot{y}_i$, $(i = 2,3,\ldots,M)$.

According to the method of nodal potentials, we form the system of equations relative to the unknown amplitudes of the nodal voltages $\dot{U}_i$. Let the harmonic probing current with the amplitude $\dot{I}_m$ is supplied on the electrode with the number m whereas the electrode with the number n is grounded, i.e. $U_n = 0$. In accordance with the method of nodal potentials, a value $\dot{I}_m$ must be assigned to first element with the number m located in the column of the currents, and the item with the number n must be deleted. Further, the column and row with the number n should be deleted from the ma-

trix $[M_Y]$, and the item with the number n should be deleted from column of the nodal potentials. As a result, we obtain the matrix system of equations

$$\left[M_{Y-}\right]\cdot\left[\dot{U}_{i-}\right]=\left[\dot{I}_{m-}\right],$$

which solution determines the unknown amplitudes of the nodal potentials $\dot{U}_i$ ($i=1,2,\ldots,M$, $i\neq n$).

The solution of the inverse problem

The inverse problem consists in the reconstruction of conductivity distribution over the area of the solid-state object under investigation by using the measurement results of the amplitude of external nodal potentials of the phantom shown in Fig. 1. Using the known amplitude of the probing current, we can restore the values of the conductivities in the circuit shown in Fig. 2.

The measurements of the amplitudes of the external nodal potentials are carried out $M/2$ times. Firstly, the probing current is supplied to the node $m=1$ while the node $n=m+M/2$ is grounded (the opposite excitation). The amplitudes of the potentials of external nodes are measured and stored. Then, the numbers of current nodes are increased by one, and measurements of the amplitudes of the nodal potentials are repeated. This procedure is performed as long as m value becomes equal to $M/2$.

Further displacement of current nodes corresponds to anti-phase excitation. Therefore, the anti-phase amplitudes of nodal potentials are acquired relative to the measured values. These additional measurements allow us to precise the values of the amplitudes of the nodal potentials. In any case, the results of the $M/2$ measurements are sufficient for the image reconstruction of the solid-state object under investigation.

Assuming that the geometry of the phantom has a form shown in Fig. 1, we can reduce the number of unknowns. For this end, we transform the formula (2) taking into account the relation (1). As a result, we obtain:

$$\dot{g}_1=R\frac{\dot{G}_M+\dot{G}_1}{2}\tan(\pi/M)=(\dot{y}_M+\dot{y}_1)\cdot\frac{\tan(\pi/M)}{\cot(2\pi/M)};$$

$$\dot{g}_i=R\frac{\dot{G}_{i-1}+\dot{G}_i}{2}\tan(\pi/M)=(\dot{y}_{i-1}+\dot{y}_i)\cdot\frac{\tan(\pi/M)}{\cot(2\pi/M)};$$

$$i=2,3,\ldots,M.$$

Let us introduce the coefficient $K=\cot(2\pi/M)/\tan(\pi/M)$. Then we get

$$\frac{\dot{y}_1}{\dot{g}_1}=K-\frac{\dot{y}_M}{\dot{g}_1},\quad \frac{\dot{y}_i}{\dot{g}_i}=K-\frac{\dot{y}_{i-1}}{\dot{g}_i},\quad (i=2,3,\ldots,M). \quad (4)$$

Thus, it is possible to use as the unknowns the relationships of conductivities $\dot{y}_M/\dot{g}_1$ and $\dot{y}_{i-1}/\dot{g}_i$, where $i=2,3,\ldots,M$, instead of their absolute values. As far as the number of unknowns is equal M, and the number of measurements is equal $M/2$, it is necessary to form two equations for each measurement. According to the scheme shown in Fig. 2, we can write the equations coupling the two adjacent nodes with numbers $m+1$ and $m+2$ as well as two diametrically opposite nodes with numbers $m+1$ and $n+1$, respectively

$$\begin{aligned}\frac{\dot{I}_{m+1}}{\dot{g}_{m+1}}-\frac{\dot{I}_{m+2}}{\dot{g}_{m+2}}&=\dot{U}_{m+1}-\dot{U}_{m+2};\\ \frac{\dot{I}_{m+1}}{\dot{g}_{m+1}}-\frac{\dot{I}_{n+1}}{\dot{g}_{n+1}}&=\dot{U}_{m+1}-\dot{U}_{n+1}.\end{aligned} \quad (5)$$

The amplitudes of the currents in equation (5) are determined by the amplitudes of the potentials of external nodes and by the conductivities of the external branches:

$$\dot{I}_{m+1}=\dot{y}_m\left(\dot{U}_m-\dot{U}_{m+1}\right)-\dot{y}_{m+1}\left(\dot{U}_{m+1}-\dot{U}_{m+2}\right),$$

$$\dot{I}_{m+2}=\dot{y}_{m+1}\left(\dot{U}_{m+1}-\dot{U}_{m+2}\right)-\dot{y}_{m+2}\left(\dot{U}_{m+2}-\dot{U}_{m+3}\right),$$

$$\dot{I}_{n+1}=\dot{y}_{n+1}\left(\dot{U}_{n+2}-\dot{U}_{n+1}\right)-\dot{y}_n\dot{U}_{n+1}.$$

Substituting the expressions for the amplitudes of the currents in relation (5) and using formulas (3) and (4), we obtain:

$$\begin{aligned}&\left(\dot{U}_m-\dot{U}_{m+2}\right)\frac{\dot{y}_m}{\dot{g}_{m+1}}-\left(\dot{U}_{m+1}-\dot{U}_{m+3}\right)\frac{\dot{y}_{m+1}}{\dot{g}_{m+2}}=\\ &=\dot{U}_{m+1}-\dot{U}_{m+2}+\frac{\dot{U}_{m+1}-2\dot{U}_{m+2}+\dot{U}_{m+3}}{K};\end{aligned} \quad (6)$$

$$\begin{aligned}&\left(\dot{U}_m-\dot{U}_{m+2}\right)\frac{\dot{y}_m}{\dot{g}_{m+1}}+\dot{U}_{n+2}\frac{\dot{y}_n}{\dot{g}_{n+1}}=\\ &=\dot{U}_{m+1}-\dot{U}_{n+1}+\frac{\dot{U}_{m+1}-\dot{U}_{m+2}-\dot{U}_{n+1}+\dot{U}_{n+2}}{K}.\end{aligned} \quad (7)$$

Substituting the values of the amplitudes of the nodal potentials measured at current nodes with numbers $m=1,2,\ldots,M/2$ and $n=m+M/2$ in equations (6) and (7) we obtain a system of linear algebraic equations. Solving this system, we find the values of unknown relationships $\dot{y}_M/\dot{g}_1$ and $\dot{y}_{i-1}/\dot{g}_i$, where $i=2,3,\ldots,M$. Then, using the formula (4), we calculate the ratios $\dot{y}_i/\dot{g}_i$ ($i=1,2,\ldots,M$).

To determine the values of conductivities $\dot{g}_i$ ($i=1,2,...,M$), we apply the Kirchhoff's first law to the nodes with numbers m and n. As a result, we obtain the following expressions:

$$\dot{g}_m\left[-\frac{\dot{y}_{m-1}}{\dot{g}_m}\dot{U}_{m-1}+\dot{U}_m\left(1+K+\frac{\dot{y}_m}{\dot{g}_{m+1}}\right)-\right.$$
$$\left.-\dot{U}_{m+1}\left(1+K+\frac{\dot{y}_m}{\dot{g}_m}\right)+\frac{\dot{y}_{m+1}}{\dot{g}_{m+1}}\dot{U}_{m+2}\right]=\dot{I}_m;$$
$$m=1,2,\ldots,M/2, \quad (8)$$

$$\dot{g}_n\left[\frac{\dot{y}_{n-1}}{\dot{g}_n}\dot{U}_{n-1}+\dot{U}_{n+1}\left(1+K+\frac{\dot{y}_n}{\dot{g}_n}\right)-\frac{\dot{y}_{n+1}}{\dot{g}_{n+1}}\dot{U}_{n+2}\right]=\dot{I}_m;$$
$$n=M/2+1,\ldots,M. \quad (9)$$

Using the expressions (8) and (9), we find the values of $\dot{g}_i$ ($i=1,2,...,M$). Then, we determine all the values of $\dot{y}_i$ and $\dot{g}_i$ ($i=1,2,...,M$) according to the previously found relations $\dot{y}_M/\dot{g}_1$, $\dot{y}_{i-1}/\dot{g}_i$ ($i=2,3,...,M$) and $\dot{y}_i/\dot{g}_i$ ($i=1,2,...,M$). Finally, using the formula (3), we calculate the values of conductivity and relative dielectric constant of each finite element (Fig. 1):

$$\sigma_i=\frac{2}{R}\mathrm{Re}\left(\dot{y}_i\tan\frac{2\pi}{M}\right);\ \varepsilon'_i=\frac{2}{R\omega\varepsilon_0}\mathrm{Im}\left(\dot{y}_i\tan\frac{2\pi}{M}\right);$$
$$(i=1,2,...,M).$$

The results of numerical investigations

Computer studies of equivalent parameters of solid-state objects were performed in a mathematical environment Matlab 7.0. Investigations were performed for cases of direct and inverse problems. For all calculations, the amplitude of the probing current was assumed to be $I_m=1$ mA. The results of calculations for the basic values of specific conductivity $\sigma=6$ mS/m and relative dielectric constant $\varepsilon'=80$ at five frequencies (10, 50, 100, 200, 300 kHz) are presented below.

By the direct problem solving, the distributions of the amplitudes $|U(\phi)|$ and phases $\varphi_U(\phi)$ of the potentials on the outer boundary of the phantom shown in Fig. 1 (ϕ is an azimuth coordinate) were calculated. The distributions of specific conductivity $\sigma(\phi)$ and relative dielectric constant $\varepsilon'(\phi)$ on the finite elements of the phantom were considered.

The calculation results showed that for the given values of $\sigma(\phi)$ and $\varepsilon'(\phi)$, the distributions $|U(\phi)|$ are almost independent of frequency. In the distributions of $\varphi_U(\phi)$, the lower value is changed. It is completely determined by the phase relation between the values σ and $j\omega\varepsilon_0\varepsilon'$ at the given frequency. The general behavior of $\varphi_U(\phi)$ is almost independent of frequency. So, it is advisable to display the distributions $|U(\phi)|$ and $\varphi_U(\phi)$ only at the frequency 300 kHz.

When solving the inverse problem of the phantom reconstruction, the restored values of conductivity $\sigma_c(\phi)$ and relative permittivity $\varepsilon'_c(\phi)$ of the material of the solid-state crystal are determined. The results of the inverse problem solution using the distributions $\dot{U}(\phi)$ obtained on the stage of the direct problem resolution show that the recovered values of conductivity $\sigma_c(\phi)$ and relative permittivity $\varepsilon'_c(\phi)$ are in good agreement with the given values.

Whereas measuring devices operate with some error, it is advisable to restore the parameters of the finite elements using the roughening of the calculation results of the amplitude $|U(\phi)|$ and phase $\varphi_U(\phi)$ characteristics. The following results are obtained for the relative errors of reconstructed values of the conductivity $[\sigma_c(\phi)-\sigma(\phi)]/\sigma(\phi)$ and relative dielectric constant $[\varepsilon'_c(\phi)-\varepsilon'(\phi)]/\varepsilon'(\phi)$ with roughening of values $|U(\phi)|$ and $\varphi_U(\phi)$ calculated at the direct problem solution to relative errors 0.1 and 0.5 percent.

Fig. 5 — Fig. 12 show the calculated characteristics for the four phantoms that contain $M=32$ finite elements. The characteristics of the homogeneous phantom *1* with the basic values of σ and ε' are presented in Fig. 5 and Fig. 6. Fig. 7 and Fig. 8 illustrate the characteristics of the phantom *2*, that differs from the phantom *1* by the presence of the sector of angles $\phi=79$—110 degrees with the conductivity of 10 mS/m. Characteristics of the phantom *3*, that differs from the phantom *1* because its conductivity is distributed according to the law $\sigma_i=\sigma\{1+\cos^2[(i-1)\pi/M]\}/2$, are shown in Fig. 9 and Fig. 10. Fig. 11 and Fig. 12 display the characteristics of the phantom *4*, that differs from the phantom *1* because its relative permittivity is distributed according to the law $\varepsilon'_i=40\{1+\cos^2[(i-1)\pi/M]\}$.

Fig. 5, Fig. 7, Fig. 9 and Fig. 11 illustrate the distributions $|U(\phi)|$ and $\varphi_U(\phi)$ calculated at the rotation of the current electrodes onto 360 degree with the step $2\pi/M$. Fig. 6, Fig. 8, Fig. 10 and Fig 12 show the relative errors of the reconstructed values $\sigma_c(\phi)$ and $\varepsilon'_c(\phi)$ for the homogeneous phantom.

The amplitude characteristics of the phantoms *1* and *4*, in which the conductivity does not change over the phantom area are practically identical. At the same time, the amplitude characteristics of the phantoms *2* and *3* have unequal distribution and change the lines curvature.

It should be also noted that the homogeneous phantom has almost linear phase characteristic $\varphi_U(\phi)$. At the appearance of any discontinuity in the plane of the

phantom, the phase characteristic becomes nonlinear. For the phantom *2* having a lumped discontinuity, the azimuth of the node on the phase characteristic corresponds to the azimuthal position of the discontinuity.

The error of the reconstruction depends on the frequency and the parameters of the discontinuity. For the phantom *2*, the azimuth of maximum errors $\sigma_c(\phi)$ and $\varepsilon'_c(\phi)$ and the azimuthal position of the discontinuity are almost identical.

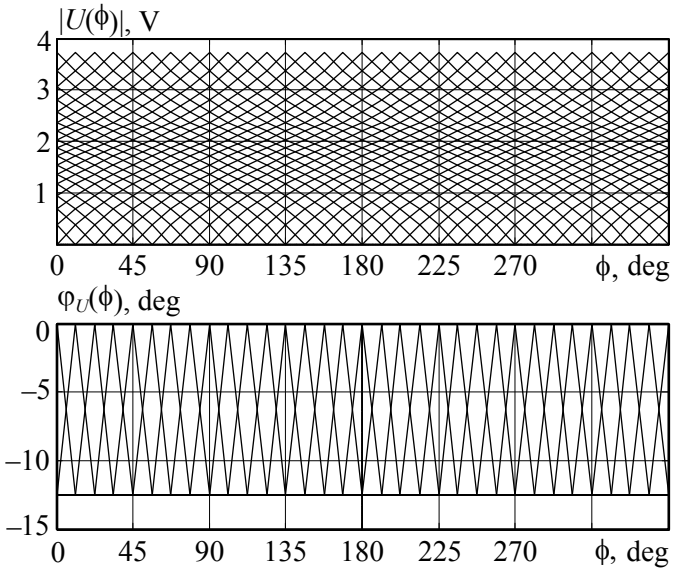

Fig. 5. Phantom *1*: The distributions of amplitudes and phases of the nodal potentials on the outer boundary at the frequency 300 kHz.

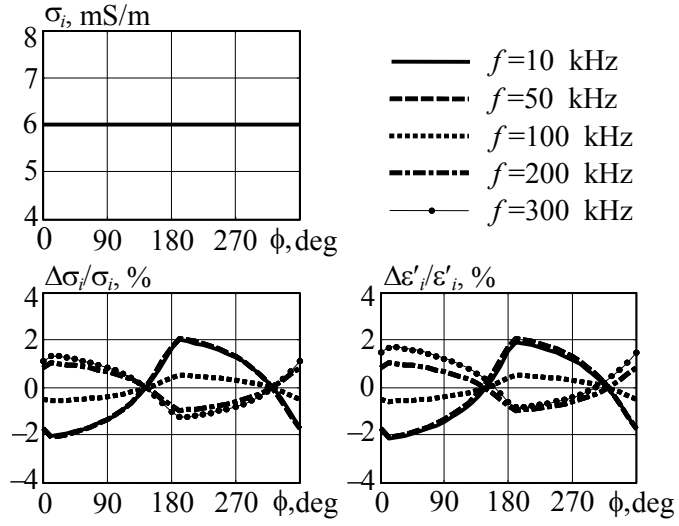

Fig. 6. Phantom *1*: The relative error of roughening of the potentials is 0.1 %.

In respect of phantoms *3* and *4*, it should be noted that the character of the variation of reconstruction errors corresponds to the character of the changes σ or ε'. The reconstruction error of the relative dielectric constant changes a sign in the vicinity of the azimuth correspond to the azimuth of maximum or minimum of the function that describes a behavior of the dielectric constant.

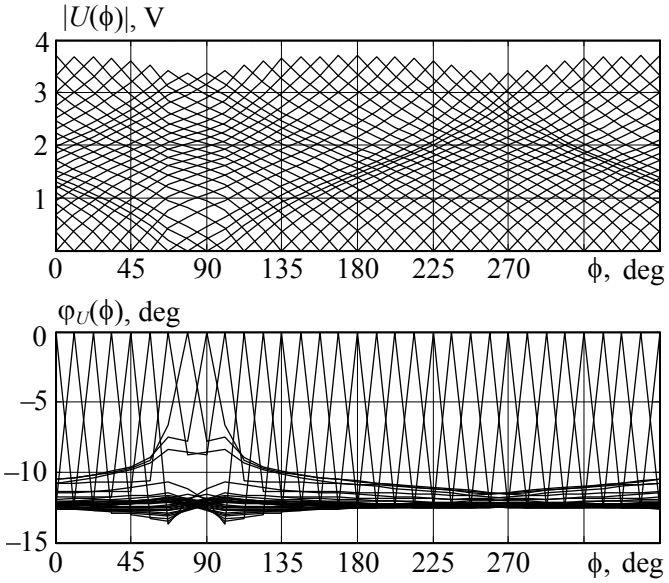

Fig. 7. Phantom *2*: The distribution of amplitudes and phases of the nodal potentials on the outer boundary at the frequency 300 kHz.

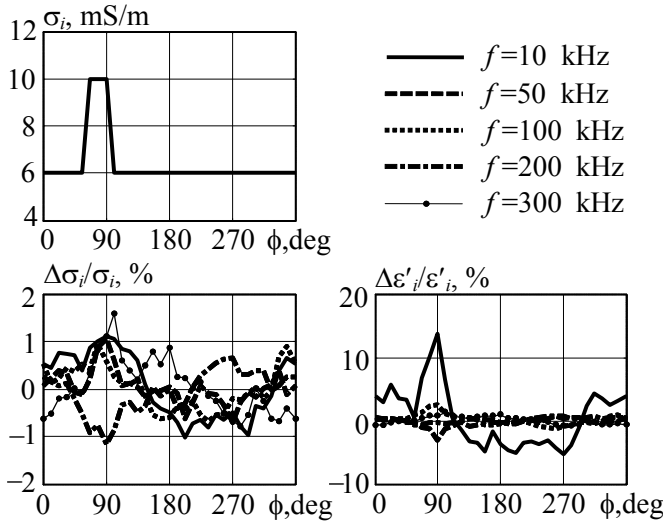

Fig. 8. Phantom *2*: The relative error of roughening of the potentials is 0.1 %.

It can be seen that the errors shown in Fig. 6 and Fig. 8 are minimal in the vicinity of the frequency 100 kHz. At low frequencies, the roughening of the phase characteristic of potentials makes the main contribution to the reconstruction error.

At these frequencies, this contribution is small and does not exceed the units of degrees. The average value

of the reconstruction error of the phantom parameters approaches zero.

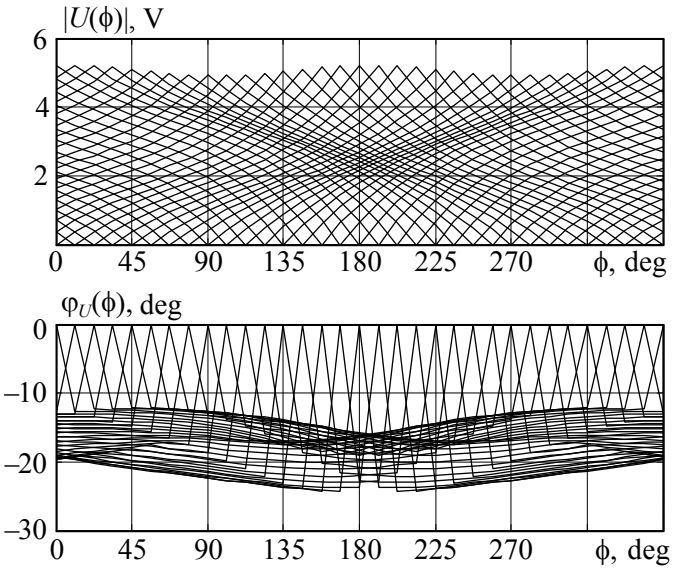

Fig. 9. Phantom *3*: The distribution of amplitudes and phases of the nodal potentials on the outer boundary at the frequency 300 kHz.

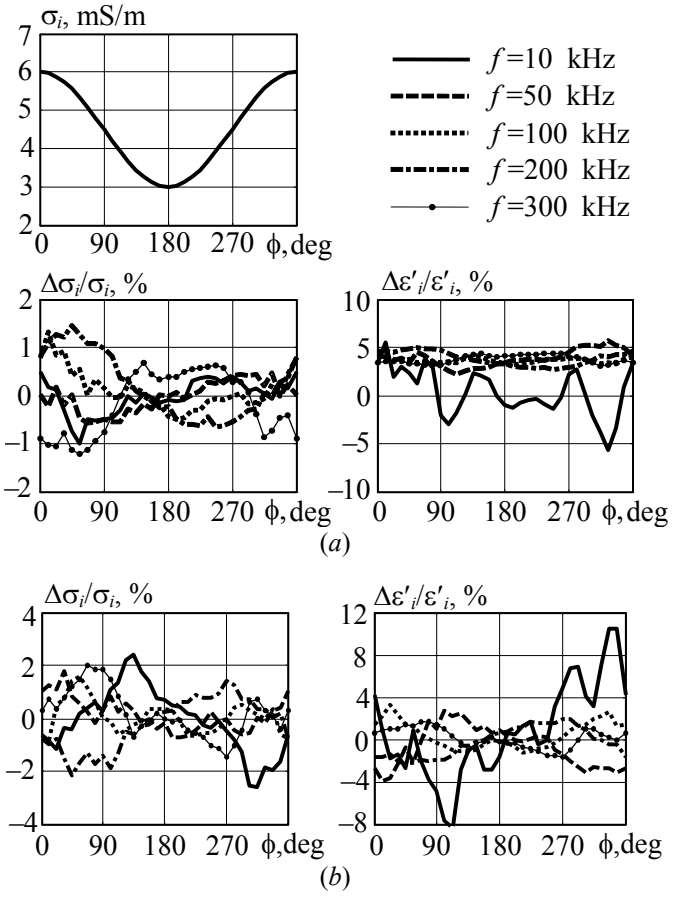

Рис. 10. Phantom *3*: (*a*) the relative error of roughening of the potentials is 0.1 %; (*b*) the relative error of roughening of the potentials is 0.5 %.

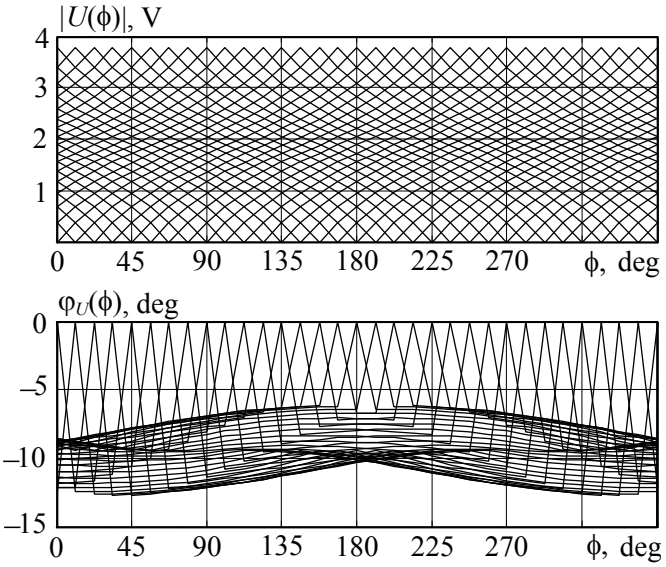

Fig. 11. Phantom *4*: The distribution of amplitudes and phases of the nodal potentials on the outer boundary at the frequency 300 kHz.

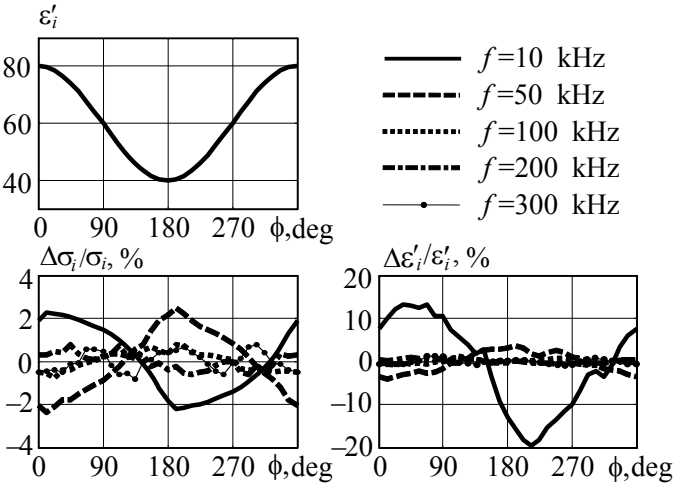

Fig. 12. Phantom *4*: The relative error of roughening of the potentials is 0.1%.

Discussion

A simple model, shown in Fig. 2, can be successfully applied to describe the processes that are concentrated outside the central region. It allows obtaining fairly correct results only for the opposite method of excitation.

To describe the processes of general form a more complex two-row model shown in Fig. 13 can be applied. The presence of a central region essentially distinguishes it from simple model shown in Fig. 2. It can be practically used under all types of multi-position excitation. This two-row model allows us to obtain a direct analytical solution of the inverse problem under certain assumptions. It is assumed here that all external

conductivities shown in Fig. 13 by mesh shading are identical and known. All the conductivities of the central region indicated by the striped and dotted shadings are also identical and known. The conductivities of the first series (they are not shaded) adjacent to the outer boundary are only unknown. A small complication of the inverse problem solving algorithm for this model allows determining the values of the conductivities of the branches located between the first and the second rows (they are shown by dotted shading). In this case, all these conductivities must have the same values.

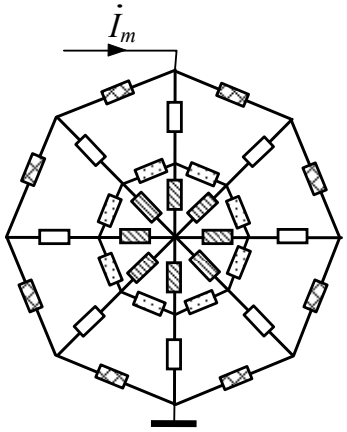

Fig. 13. Two-row model.

To obtain accurate results, the model shown in Fig. 13 needs some revision as it is confirmed by the experimental data. An adequate initial approximation when solving the complicated problems of image reconstruction of solid-state component can be derived using the model shown in Fig. 2.

The calculated distributions of the amplitudes and phases of the nodal potentials obtained by computer simulation are rounded to four significant decimal digits. In reality, the error of image reconstruction depends on the value of the measured parameter and increases with decreasing of amplitude and phase of the potentials.

Distributions of nodal potentials obtained by solving the direct problem for the case of direct current have been compared with the same ones derived in the solution of the direct electrostatic problem by finite element method [15]. The compared characteristic parameters calculated by these two methods were in good agreement.

Conclusion

The approximate model of inhomogeneous solid-state elements which allows unique analytic solution of the tomographic synthesis problem has been proposed and investigated. This solution can be used as an initial approximation when investigating the complicated objects. It can accelerate the actual process of image reconstruction, especially in cases when the object structure is not known beforehand.

References

1. Jaeger R. C., Blalock T. N. Microelectronic circuit design. ─ McGraw-Hill, 2010. ─ 1360 p.

2. Bahl I., Bhartia P. Microwave Solid Circuits Design. ─ New York: Wiley, 2003. ─ 906 p.

3. Using computerized tomography in non-destructive testing of the solid materials / M. Iovea, A. Marinescu, C. Rizescu, G. H. Georgescu // The Annual Symposium of the Institute of Solid Mechanics, Romanian Academy, Bucharest, Romania, December 15─16, 1994. ─ P. 357─364.

4. Three-dimensional electrical impedance tomography applied to a metal-walled filtration test platform / J. L. Davidson, L. S. Ruffino, D. R. Stephenson, R. Mann, B. D. Grieve, T. A. York // Measurement Science and Technology. ─ 2004. ─ Vol. 15, N. 11. ─ P. 2263─2274.

5. York T. Status of electrical tomography in industrial applications // Journal of Electronic Imaging. ─ 2001. ─ V. 10, N. 3. ─ P. 608–619

6. Muller H. Boundary extraction for rasterized motion planning / Modelling and Planning for Sensor Based Intelligent Robot Systems // World Scientific, 1995. ─ P. 41─50.

7. Electrical impedance tomography: Methods, history and applications / Edited by D. Holder. ─ Bristol: Institute of Physics Publisher, 2005. ─ 576 p.

8. Ross R. W.; Hinton Y. L. Damage diagnosis in semiconductive materials using electrical impedance measurements // Proceedings of 49th International Conference "Structures, Structural Dynamics and Materials", Schaumburg, IL, USA, April 7─10, 2008. ─ 9 p.

9. Hou T.-C., Loh K. J., Lynch J. P. Spatial conductivity mapping of carbon nanotube composite thin films by electrical impedance tomography for sensing applications // Nanotechnology. ─ 2007. ─ V. 18, N. 31 ─ P. 1─9.

10. Wang M., Dickin F. J., Mann R. Electrical resistance tomographic sensing systems for industrial applications // Chemical Engineering Communications. ─ 1999. ─ Vol. 175, N. 1. ─ P. 49─70.

11. Natterer F. The Mathematics of computerized tomography. ─ Society for Industrial and Applied Mathematics, 2001. ─ 222 p.

12. Tikhonov A. N., Arsenin V. Y. Solutions of ill-posed problems. ─ New York: Winston, 1977. ─ 288 p.

13. Electrical impedance tomography / Y. S. Pecker, K. S. Brazovskiy, V. Y. Usov, M. P. Plotnikov, O. S. Umanskiy. ─ Tomsk: NTL Publisher, 2004. ─ 192 p. [in Russian].

14. Sylvester P., Ferrari R. The finite element method for radio engineers and electrical engineers. ─ Cambridge: Cambridge University Press, 1983. ─ 228 p.

15. Guseva O. V., Naidenko V. I., Prokopenko A. P. Solution of direct problem of tomography of applied potentials // Proceedings of International Conference "Mathematical Methods in Electromagnetic Theory". ─ Kharkov, June 2─5, 1998. ─ P. 612─614.

Received in final form September 16, 2011